

Chitosan-coupled Solid Lipid Nanoparticles: tuning nanostructure and mucoadhesion

Giuseppina Sandri¹, Simona Motta², Maria Cristina Bonferoni¹, Paola Brocca², Silvia Rossi¹, Franca Ferrari¹, Valeria Rondelli, Laura Cantù^{2,*}, Carla Caramella¹, Elena Del Favero²

¹Dept of Drug Sciences, University of Pavia, Via Taramelli, 12, 27100 Pavia, Italy.

²Dept. Medical Biotechnologies and Traslational Medicine, University of Milano. LITA, Via F.lli Cervi, 93. 20090 Segrate, Italy

*Corresponding author

Prof. Laura Cantù

Dept. Medical Biotechnologies and Traslational Medicine, University of Milano. LITA, Via F.lli Cervi, 93. 20090 Segrate, Italy

Tel. 02 503.30362 / 30351 / 30326

Fax. 02 503.30365

e-mail: laura.cantu@unimi.it

Keywords: solid lipid nanoparticles, chitosan, structural analysis, mucoadhesion

Running Title: Structure and mucoadhesion of chitosan-coupled SLNs

Abstract

Solid Lipid Nanoparticles (SLNs) composed of biodegradable physiological lipids have been widely proposed as efficient drug delivery systems, also for ophthalmic administration. Recently, chitosan-associated-SLNs have been developed to further improve the residence time of these colloidal systems in the precorneal area by means of mucoadhesive interaction. In the present study, a one-step preparation protocol was used aiming both at scale-up ease and at stronger coupling between chitosan and SLNs. The resulting particles were chitosan associated-SLNs (CS-SLNs). These nanoparticles were characterized, as compared to both the chitosan-free and the usual chitosan-coated ones, by applying a multi-technique approach: light, neutron and x-ray scattering, Zeta-potential, AFM, calorimetry. It was assessed that, while keeping the features of nano-size and surface-charge required for an efficient vector, these new nanoparticles display a strong and intimate interaction between chitosan and SLNs, far more settled than the usual simple coverage. Moreover, this one-step preparation method allows to obtain a strong and intimate interaction between chitosan and SLNs, firmer than the usual simple coating. This confers to the CS-SLNs an improved mucoadhesion, opening the way for a high-performing ophthalmic formulation.

1. Introduction

Solid lipid nanoparticles (SLNs) are sub-micron colloidal carriers composed of biodegradable physiological lipids with GRAS (Generally Recognized As Safe) regulatory status. Therefore SLNs are commonly considered to be less toxic than polymer-based nanoparticles. Moreover SLNs combine the advantages of colloidal systems (higher surface-to-volume ratio, protection of incorporated labile drugs from degradation, controlled release properties and improved pharmacokinetics and biodistribution) with a physical stability almost similar to that of conventional drug delivery systems.

SLN formulations have been developed for various application routes (parenteral, oral, dermal, ocular, pulmonary, rectal) and thoroughly characterized *in vitro* and *in vivo*. As for the ophthalmic administration route, SLNs have been widely proposed as efficient drug delivery systems due to small particle size (less than 1 μm), narrow size and low polydispersity, adequate bioavailability, good tolerability and compatibility with ocular tissue and absence of blurred vision (1-3). SLNs administered in the precorneal district demonstrated to be able to increase bioavailability (4). This is likely due to the small size of the SLN, allowing for increased entrapment and retention in the mucin layer covering the corneal epithelium (4). These features have emerged to be central and challenging issues for ocular drug delivery. In fact, the retention time of common formulations in the precorneal district is normally short, being subjected to eyelid movement (blinking) and removal by tears via the naso-lachrymal duct. In addition eye's barriers (epithelial, aqueous-vitreous, blood-aqueous barrier) limit the entry of topically administered drugs. Drug penetration into the anterior and posterior chambers is however necessary to treat some ophthalmic diseases such as glaucoma or uveitis (5).

Recently, chitosan-associated-SLNs (CS-SLNs) have been developed to further improve the residence time of SLNs colloidal systems in the precorneal area, via mucoadhesive interaction (6). The peculiar properties of chitosan, a cationic polysaccharide, are exploited. In fact, chitosan shows good mucoadhesion properties and enhances drug penetration across various epithelia (7, 8). These features would further prevent removal of nanoparticles from the eye while simultaneously favouring internalization in the corneal cells. CS-SLNs demonstrated to be biocompatible and to enhance permeation/penetration of a loaded drug, namely cyclosporin A, in both *in vitro* (RCE cell substrate) and *ex vivo* (excised cornea) models. CS-SLNs interaction with the corneal surface, required for internalization/uptake, is favoured by the presence of positively-charged chitosan. This aspect could be exploited in the treatment of eye pathologies, the cornea acting as a reservoir, maintaining a constant drug level and thus decreasing the number of required instillations.

In order to maximise the potentiality of chitosan, a one-step protocol has been here proposed aimed

to closer coupling with SLNs, avoiding simple coating. CS-SLNs were prepared by means of high-shear homogenization and ultrasound method (9) optimized previously (6, 10). The preparation process was based on one-step emulsion: the lipid phase (Compritol[®] 888 ATO) was emulsified with an aqueous phase containing chitosan and surfactants (Pluronic[®] F68 and Tween[®] 80).

In the present work, the structure of chitosan-based SLNs has been studied, in order to identify the peculiar features induced by the type of chitosan association, either as simple coverage of preformed SLNs or early participating to the nanoparticle formation. (6). For a complete structural characterization, different techniques were applied on naked-SLNs (prepared without chitosan, hereafter SLNs), on chitosan-coated-SLNs (hereafter CS-c-SLNs) and on new CS-SLNs. On the whole particle length-scale, the particles size, the surface charge and the particles morphology were assessed by Dynamic Light Scattering (DLS) and Zeta-Potential (ZP) measurements and Atomic Force Microscopy (AFM), respectively. The shape and the internal structure of the nanoparticles were studied by Small-Angle X-ray and Neutron Scattering (SAXS and SANS). Wide-Angle X-ray Scattering (WAXS) was applied to get hints on the very local structure (Ångstrom lengthscale). Parallel Differential Scanning Calorimetry (DSC) measurements were performed to assess the thermotropic behaviour of the nanoparticles. This multi-technique approach was essential to deeply investigate the differences in the nanoparticles structure that could result in significant differences in their mucoadhesive properties.

Finally, mucoadhesion properties were evaluated by Turbidimetry (T) and compared for the three different systems.

2. Materials and methods

2.1 Materials

Glyceryl Behenate, Compritol[®]888 ATO, a kind gift from Gattefossè (Milan, Italy), was chosen as lipid. Poloxamer188 (Plu) (Pluronic[®]F68, BASF, Cesano Maderno, Italy) and Tween[®]80 (T80, Fluka, Milan, Italy) were used as surfactants. Chitosan (CS) (MW 251 kDa, assessed by viscosimetric evaluation (11); deacetylation degree: 98%) (Giusto Faravelli, Milan, Italy) was hydrated in distilled water by adding a stoichiometric amount of HCl and then freeze-dried.

2.2 Methods

2.2.1 SLNs preparation

Chitosan-associated-SLNs (CS-SLNs) were prepared by means of high shear homogenization and ultrasound method (9) optimized previously (6). The lipid phase, Compritol[®]888 ATO (C888) (100

mg), was melted at 85°C. The aqueous phase was based on Pluronic®F68 (50 mg) and Tween®80 (50 mg) dissolved in 12.5 ml of a 1% chitosan hydrochloride solution (125 mg of chitosan as base hydrated by using hydrochloric acid aqueous solution 0.18 N), and heated to 85°C. The aqueous phase (12.5 ml) was poured into the lipid phase under homogenization at 24000 rpm for 5 min with UltraTurrax (T25, IKA-Werke GmbH, Germany). The solution was then diluted with 12.5 ml bidistilled water at 4°C and kept at -20°C for 10 min. CS-SLNs were submitted to ultrasound treatment (ultrasound frequency 37 kHz) (Elmasonic S80 H, Elma Hans Schmidbauer GmbH & Co, Singen, Germany) for 10 min to avoid agglomeration during re-crystallization. They were kept at 4°C until measurement, at least for one day. All samples were measured within two weeks from preparation.

Chitosan-coated-SLNs (CS-c-SLNs) were prepared using an analogous procedure, using the same lipid phase. The aqueous phase, containing Pluronic®F68 and Tween®80, was chitosan free. Chitosan was added afterwards, after hot emulsification of SLNs, upon dilution with a 1% w/w chitosan solution at 4°C, instead of water.

Naked-SLNs (SLNs) were prepared according to the previously described procedure (10), including high-shear homogenization and ultrasound treatment, with the same components except for chitosan.

2.2.2 Particle size measurements

Laser light scattering measurements were carried out on a standard apparatus (SM200, Brookhaven Instruments Co, Holtsville, New York, USA) equipped with an Argon ion laser operating on the 514 nm green line (Lexel, Fremont, CA, USA) and a thermostat. Samples were properly diluted, typically 1:15 with respect to the original solutions, in order to avoid multiple scattering, and inserted into the measuring cell. Water was accurately filtered (on 0.2 µm pore size polycarbonate membranes) in order to avoid dust contamination.

DLS experiments were performed on each sample.

The correlation function of the scattered light, was collected at 90° scattering angle, at T = 25°C. At least three measurements were performed for each sample.

The correlation function analysis was performed both with the Cumulant Method (12), giving the particle average size and polydispersity index, and with NNLS (Non-Negatively constrained Least Squares) (13), estimating the particle size distribution.

2.2.3 Zeta Potential (ZP) measurements

The ZP of nanoparticles was calculated (as described in the instruction manual for ZetaPALS, Zeta Potential Analyzer) measuring the electrophoretic mobility of dispersed particles at 25°C, by using a standard Zeta PALS instrument (Brookhaven Instruments Co, Holtsville, New York, USA).

Measurements were performed on each system at three concentrations: a) as from the preparation protocol b) after 1:2 dilution and c) after 1:15 dilution with deionized and filtered (0.2 μm) water (pH 6.5). Ten repetitions were made on each sample.

2.2.4 Atomic Force Microscopy (AFM) measurements

Samples were mounted onto a Multimode AFM with a NanoScope V system (Veeco/Digital Instruments) operating in Tapping Mode, using standard phosphorus-doped silicon probes (T: 3.5 - 4.5 μm , L: 115 - 135 μm , W: 30 - 40 μm , f_0 : 311 - 364 kHz, K: 20 - 80 N/m) (Veeco). The original samples were diluted 1:200 with MilliQ filtered (0.2 μm) water. 60 μl of diluted sample were deposited on a freshly-stripped mica surface, with circular shape (diameter 10 mm) and left for 10 seconds. Then, the surface was thoroughly rinsed with deionized filtered water and subsequently dried under a gentle flux of nitrogen. Two-to-five different fields of the same deposited sample were observed. The processing of the AFM images was performed with the instrument built-in program (Nanoscope Veeco).

2.2.5 Differential Scanning Calorimetry (DSC) Measurements

Calorimetric measurements were performed on an updated version of the MASC instrument, operated in the DSC mode (14). Weighted amounts of each sample ($\sim 200 \mu\text{l}$, CS-SLNs, CS-c-SLNs and SLNs in aqueous solution) were put in glass capillaries, and then carefully sealed. Also a small amount of pure Compritol[®], in powder form, was sealed in a glass capillary. Capillaries were weighted before and after each measurement. Samples were evaluated in the 37 - 77°C temperature range, at a scan rate of 1°C/min, in heating and cooling modes. Some cooling scans were performed after long equilibration (2 hours) at 77°C, in order to ensure complete fusion of the nanoparticle core. Several sequential heating and cooling scans were performed.

2.2.6 Small Angle (SAXS) and Wide Angle (WAXS) X-ray Scattering Measurements

SAXS and WAXS experiments were performed at the ESRF high-brilliance synchrotron facility (Grenoble, FR) on the ID02 beamline, in the range of momentum transfer $q = 0.03 - 6 \text{ nm}^{-1}$ for SAXS and $q = 7.5 - 55.5 \text{ nm}^{-1}$ for WAXS (wavelength of the incident beam $\lambda = 0.1 \text{ nm}$). Very small amounts of the SLNs suspensions ($\sim 30 \mu\text{l}$) were put into plastic capillaries (KI-BEAM – ENKI srl, Italy), with 98% X-ray transmittance, and measured. Single exposures were of 0.1 s, and no radiation damage of the samples occurred. Measurements were performed at room temperature. Standard protocols for data reduction, subtraction and analysis were followed.

2.2.7 Mucoadhesion measurements

Mucoadhesion measurements were performed by means of the Turbidimetric method (15).

Turbidimetric measurements were carried out using a spectrophotometer (UV-vis Lambda 25, Perkin Elmer, Milan, I) operating at $\lambda = 500$ nm (according to Eur Pharm 6th Ed). Gastric mucin (porcine type I-S, Sigma Aldrich, Milan, Italy) was dispersed in distilled water under mild stirring at room temperature at the following concentrations: 0.1; 0.25; 0.5; 0.75; 1.0 % (w/v). Aliquots of the various mucin solutions were then mixed with the SLNs suspensions, 1:1 in volume. The SLN-mucin mixtures were equilibrated for 30 min at room temperature before turbidimetric measurement. Turbidity of individual mucin and SLNs solutions was also measured.

The turbidity values were elaborated according to the method described by He et al. (16). The effective absorbance (A) of the SLN-mucin mixtures, was compared to the theoretical absorbance (A_{theor}) calculated by adding the individual absorbance values of the mucin and SLNs solutions. The difference in absorption ($\Delta A = A - A_{\text{theor}}$) is taken as a measure of the interaction between mucin and the SLNs, namely $\Delta A \cong 0$ if no interaction occurs, while if $\Delta A \gg 0$, a strong interaction between mucin and the SLNs is inferred. The per cent variation, $\Delta A\% = \Delta A/A_{\text{theor}} \times 100$, was also evaluated.

3. Results and discussion

3.1 Charge of nanoparticles: ZP evaluation

SLNs bear negative surface charge. This is due to the presence of Poloxamer188. In fact, Pluronic[®]F68 solution shows a negative Z-potential (~ -12 mV) as well as SLNs, (~ -15 mV), a value that does not depend on concentration. Differently, Tween[®]80 in solutions forms electrically neutral aggregates. Chitosan-based nanoparticles, CS-SLNs and CS-c-SLNs, bear positive surface charge, typical of the reentrant condensation regime (17, 18) indicating that association of the positively charged chitosan to the nanoparticles has occurred, exceeding neutralization of their negative charge. A small population of particles with low negative surface charge was also detected, in largely minor amount. In Fig.1 the ZP measured for SLNs, CS-SLNs and CS-c-SLNs, are reported, for three concentrations, as from the preparation protocol and upon 2-fold and 15-fold dilution. It can be seen that the positive ZP of chitosan-based nanoparticles tends to increase upon dilution and, more interestingly, that the charge of CS-SLN is systematically higher than that of CS-c-SLN (ZP ~ 40 mV and ZP ~ 25 mV, respectively at the concentration of preparation protocol). This is a point of great interest in view of the application of CS-SLN for ophthalmic administration, being the improvement of mucoadhesion related to nanoparticle charge, a favourable feature.

3.2 Particle size and morphology evaluation: DLS and AFM results.

The average size and polydispersity for naked and chitosan based systems were measured by DLS.

The cumulant analysis shows that the presence of chitosan clearly induces an increase in the overall average size of particle population as compared to the naked SLN, of the order of 40%, passing from 140 ± 10 nm to 200 ± 30 nm. For all the systems, the polydispersity index is around 0.30.

NNLS analysis on light scattering data reveals that in the chitosan-free system most of the particles belong to a small-size population, with average diameter ~ 40 nm, nicely reproducible on different preparations. This majority population is also clearly appearing in the AFM image of Fig. 2. The higher value of the overall average size, as determined by the cumulant analysis, is affected by the presence of second population, very exiguous in number but larger in size, and then highly contributing to the scattering and to the overall polydispersity.

In both chitosan-based systems, SLNs are around 150 nm in size, as estimated by NNLS analysis. The interaction between lipids, surfactants and chitosan leads to the formation of globular particles where a rather stiff core is enveloped by a jelly cover. The morphology of such nanoparticles is visible in the AFM picture of Figure 3. A very small population of very large aggregates, >500 nm by NNLS, is shown by AFM to be constituted of residual chitosan threads. A small population of particles with size and morphology very similar to those of the naked SLN, suggests the presence of some residual chitosan-free nanoparticles.

3.3 Thermotropic behaviour: Differential Scanning Calorimetry

The predominant contribution in the DSC calorigram of the SLNs is given by the Compritol[®] 888ATO, which is an atomized mixture of glycerol mono- (18% bw), di- (52% bw) and tri-behenate (28% bw) (Ph. Eur.). Along the melting process, see Fig. SM1 of Supporting Material, the heterogeneous and polymorphic nature of Compritol[®] results in a complex DSC thermogram, showing three enthalpic peaks in the temperature range $70-75^{\circ}\text{C}$, the lowest being attributed to triglyceride, the highest to the mono-glyceride component (19). A more detailed description is provided in the Supporting Material.

Figure 4 reports the DSC thermograms (second heating scan) of all SLNs samples. Results show that calorimetric peaks are present in all the systems, due to the melting transition of the lipid core within the particles. This indicates that Compritol[®] still keeps some crystalline structure within the nanoparticles, undergoing the melting process. On the other hand, melting occurs at lower temperatures as compared to the bulky Compritol[®], the whole process completing $\sim 5^{\circ}\text{C}$ lower, showing that its confinement within the small volume of the interior of nanoparticles induces higher disorder of the lipid phase. It is also interesting to note that, while for bulky Compritol[®] subsequent heating (cooling) runs are superimposable, except for the first ones (see Fig. SM1 in Supporting

Material), the Compritol[®] hosted inside nanoparticles undergoes progressive structural rearrangement, seemingly gradually isolating the three components from each other, maybe responding to nanoscale spatial confinement (see Fig. SM2 in Supporting Material). The DSC profiles of the nanoparticles systems are reported in Figure 4, showing that the fragmentation of Compritol[®] in nanoparticles is much more effective than the addition of chitosan to nanoparticles and the specific preparation protocol, resulting in rather similar profiles, all different from that of the bulk Compritol[®]. The finding that, even in the core of nanoparticles, the lipid phase maintains some ordered structure is of extreme importance, in view of both loading significative amounts of different lipophilic drugs and their subsequent efficient release.

3.4 Local structure: X-ray measurements

To investigate the internal structure of nanoparticles, both SAXS and WAXS measurements were performed on the different SLNs and on their main components. In particular, high brilliance ID02 beamline allowed obtaining detailed information on the internal structure of nanoparticles down to the very local scale, corresponding to the short reticular distances between the hydrocarbon chains of the lipid core (WAXS). Glycerides mixtures like Compritol[®], exhibit a complex polymorphism, due to multiple options in the lateral packing of fatty acids chains. In fact, a polymorphic behaviour is often shown by long-chain compounds (20) that, in general, crystallize in two or three different phases. The WAXS spectrum of Compritol[®] is reported in Figure 5a): two major peaks are visible at $q = 15 \text{ nm}^{-1}$ and $q = 16.5 \text{ nm}^{-1}$. Those peaks correspond to the characteristic distances 4.2 \AA (star) and 3.8 \AA (circle) of the known crystallographic α -subcell of glycerides at room temperature (21)

Even when Compritol[®] is fragmented into nanometric portions embedded in nanoparticles in dilute solution, the WAXS spectra clearly show the liquid-crystal structure of the lipid phase, in agreement with DSC results. Fig. 5 b) and c) reports the WAXS spectra of nanoparticles in the crucial q -region, where the two major peaks at $q = 15 \text{ nm}^{-1}$ (star) and $q = 16.5 \text{ nm}^{-1}$ (circle) are still visible, typical of the α -subcell, for both the chitosan-free and the chitosan-based nanoparticles. Still, an interesting difference is seen in the local structure, discriminating chitosan-based nanoparticles from chitosan-free. In fact, in the case of chitosan-free SLNs (Figure 5b)), the observed crystallographic structure corresponds perfectly to that of Compritol[®] at room temperature. Reversely, in the case of Cs-SLNs and CS-c-SLNs ((Fig.5 panel c) an additional peak rises at $q = 13.6 \text{ nm}^{-1}$. This reveals that the local structure of chitosan-based nanoparticles core is not homogeneous. Only part of the lipid assumes the same structure found in SLNs and Compritol[®], while a fraction of it arranges in a looser structure, with characteristic distance of 4.6 \AA (arrow in figure 5c). This local structure is similar to that observed at higher temperature (around $63 \text{ }^\circ\text{C}$) during a cooling process of pure Compritol[®], starting

from the melted compound, where the corresponding β' subcell has the same characteristic distance of 4.6 Å.

Those results indicate that the presence of chitosan affects the organization of the solid core, loosening its crystalline tightness, whatever the preparation protocol for chitosan addition, a feature that can be of importance when a lipophilic drug has to be encapsulated in the SLNs.

SAXS parallel measurements were performed on both chitosan-free and chitosan-based SLNs systems and on their main components, pure Compritol[®] and chitosan (in water solution). The SAXS spectra of the SLNs systems are shown in Figure 6 in the region $q = 0.03 - 2.65 \text{ nm}^{-1}$, vertically shifted for better comparison, presenting a profile well corresponding to that of core-shell nanoparticle systems. Features arising from main components can be identified. The SAXS spectrum of pure Compritol[®] displays the features of the expected lamellar phase. In Figure 6, only the main peak at $q = 1 \text{ nm}^{-1}$ is reported (bottom), corresponding to a characteristic distance $d = 6.2 \text{ nm}$, in agreement with literature results (21). This structure cannot be kept as such in the nanometric confined core of the nanoparticles, nonetheless a broader peak, at the same characteristic distance of 6.2 nm, is visible in all the SLNs spectra, both chitosan-free and chitosan-based, in fact all hosting a Compritol[®] core. Moreover, in the chitosan-based systems, a broad peak is visible, at $q \sim 0.4 \text{ nm}^{-1}$. The supramolecular organization of chitosan has been extensively studied (22) and it is typical of polyelectrolytes. In Figure 6 the experimental spectrum of free chitosan in the region of the peak at $q = 0.43 \text{ nm}^{-1}$ (second from bottom) allows for comparison. The broad peak in chitosan-based nanoparticles is likely the contribution of residual free chitosan, already detected by means of DLS and AFM results. Moreover, the intensity profiles differ in the low q region: CS-SLNs and CS-c-SLNs profiles are steeper than that of the chitosan-free SLNs. X-ray results indicate that the presence of chitosan, in both chitosan-based systems, while preserving the main features of the internal structure of the nanoparticles, interferes with the external shell, modifying the contrast profile and the overall size of the particle.

3.5 Mucoadhesion properties

To evaluate and compare the mucoadhesion performance of chitosan-based nanoparticles, they were admixed with different amounts of mucin I-S, in the range 0.25-1%, and the excess absorbance ΔA of the mixture was measured. Results are reported in Figure 7, in terms of the percent excess absorbance $\Delta A\%$. The values obtained on admixing pure chitosan to mucin, at the same concentration of components, is also reported.

Chitosan is well-known as mucoadhesive polymer towards not only ophthalmic tissues but also other mucosal districts such as buccal, vaginal and nasal mucosae (23-25). To better characterize chitosan SLN systems and understand how the type of interaction between chitosan and SLN could influence

the mucoadhesion behavior, distilled water was chosen as medium to avoid a possible interference effect of ions and ionic strength on chitosan mucoadhesive properties (26). In particular, the presence of anions could shield chitosan chains affecting polymer chain conformation and giving a contracted coil, less prone to form mucoadhesive joints. Moreover the presence of ions and high ionic strength could prevent chitosan to form a deep interpenetration with mucin chains. These events could render difficult the comprehension of the contribution given by chitosan interaction with mucin.

Admixing chitosan-free SLNs did not result in a positive excess absorbance, as expected due to their negative surface charge.

All over the explored concentration range, CS-SLNs present higher values of $\Delta A\%$ with respect to the CS-c-SLNs, thus displaying higher mucoadhesion performance in all conditions. Best mucoadhesive properties are shown in the intermediate range of mucin concentration (0.5-0.75 w/v), suggesting that optimal coverage of nanoparticles may occur. Noteworthy, in this range of concentration, an inversion in mucoadhesion efficiency is seen between the CS-SLNs and pure chitosan itself. This behaviour is not observed for CS-c-SLNs. This result reveals that chitosan complexation in CS-SLNs is not limited to simple nanoparticle coverage, but rather it provides a much better exposure of chitosan charged groups to external interaction, enhancing nanoparticle adhesion performance.

4. Conclusions

In order to improve the performance of nanoparticles for drug administration in the precorneal district, few-steps preparation protocol should allow both at scale-up ease and at stronger coupling between chitosan and SLNs. Chitosan-associated-SLNs (CS-SLNs) were obtained. The physico-chemical properties of these nanoparticles with those of the usual chitosan-covered SLNs (CS-c-SLNs), a benchmark for mucoadhesive nanovectors for hydrophobic drugs, were compared. While keeping the features of nano-size and surface-charge required for an efficient vector, these new nanoparticles display a strong and intimate interaction between chitosan and SLNs, far more settled than the usual simple coverage. This confers to the CS-SLNs an improved mucoadhesion, opening the way for a high-performing ophthalmic formulation.

Acknowledgments

We thank the beamline scientists at ID02 for technical assistance, Laura Colombo for skilled advice in AFM measurements, and Elisabetta Ricci for sample preparation and performing some DLS experiments.

References

- (1) Zimmer, A.; Kreuter, J. Microspheres and nanoparticles used in ocular delivery systems. *Adv. Drug Deliv. Rev.* 1995, 16, 61-73
- (2) Seyfoddin, A.; Shaw, J.; Al-Kassas, R. Solid lipid nanoparticles for ocular drug delivery. *Drug Delivery* 2010, 17, 467-489
- (3) Iqbal, M.A.; Sahni, J.K.; Baboota, S.; Dang, S.; Ali, J. Nanostructured lipid carriers system: Recent advances in drug delivery. *J. Drug Target.* 2012, 10, 813-830
- (4) Cavalli, R.; Gasco, M.R.; Chetoni, P.; Burgalassi, S.; Saettone, M.F. Solid lipid nanoparticles (SLN) as ocular delivery system for tobramycin. *Int. J. Pharm.* 2002, 1-2, 241-245
- (5) Sandri, G.; Bonferoni, M.C.; Gokçe, E.H.; Ferrari, F.; Rossi, S.; Patrini, M.; Caramella, C. Chitosan-associated SLN: In vitro and ex vivo characterization of cyclosporine A loaded ophthalmic systems. *J. Microencapsul.* 2010, 27, 735-746
- (6) Liu, S.; Jones, L.; Gu, F.X. Nanomaterials for Ocular Drug Delivery. *Macromolecul Biosci.* 2012, 12, 608-620
- (7) Caramella, C.; Ferrari, F.; Bonferoni, M.C.; Rossi, S.; Sandri, G. Chitosan and its derivatives as drug penetration enhancers. *J Drug Del. Sci. Technol.* 2010, 20, 5-13
- (8) Zambito, Y.; Di Colo, G. Chitosan and its derivatives as intraocular penetration enhancers. *J Drug Del. Sci. Technol.* 2010, 20, 45-52
- (9) Mehnert, W.; Mäder, K. Solid lipid nanoparticles: Production, characterization and applications. *Adv. Drug Deliv. Rev.* 2001, 47, 165-196
- (10) Gokce, E.H.; Sandri, G.; Bonferoni, M.C.; Rossi, S.; Ferrari, F.; Güneri, T.; Caramella, C. Cyclosporine A loaded SLNs: Evaluation of cellular uptake and corneal cytotoxicity. *Int. J. Pharm.* 2008, 364, 76-86
- (11) Rossi, S.; Marciello, M.; Sandri, G.; Ferrari, F.; Bonferoni, M.C.; Papetti, A.; Caramella, C. Wound-dressings Based on Chitosans and Hyaluronic Acid for the Release of Chlorhexidine Diacetate in Skin Ulcer Therapy. *Pharm. Dev Technol.*, 2007, 12, 415-422
- (12) Koppel, D.E. Analysis of Macromolecular Polydispersity in Intensity Correlation Spectroscopy: The Method of Cumulants. *J. Chem. Phys.* 1972, 57, 4814
- (13) Grabowski, E.; Morrison, I. Measurements of Suspended Particles by Quasi-Elastic Light Scattering. In *Particle Size Distributions from Analysis of Quasi-Elastic Light Scattering Data*; Dahneke, B., Ed.; Wiley-Interscience: New York, 1983; 30, 113-121
- (14) Salvetti, G.; Cardelli, C.; Ferrari, C.; Tombari, E. A modulated adiabatic scanning calorimeter (MASC). *Thermochimica Acta.* 2000, 364, 11-22.
- (15) Bonferoni, M. C., Sandri, G.; Ferrari, F.; Rossi, S.; Larghi, V.; Zambito, Y.; Caramella, C. Comparison of different in vitro and ex vivo methods to evaluate mucoadhesion of glicol-palmitoyl chitosan micelles, *J. Drug Del. Sci. Technol.*, 2010, 20, 419-424
- (16) He, P.; Davis, S.S.; Illum, L. In vitro evaluation of the mucoadhesive properties of chitosan microspheres. *Int. J. Pharm.* 1998, 166, 75-88
- (17) Grosberg, A. Y.; Nguyen, T. T.; Shklovskii, B. I. Colloquium: The physics of charge inversion in chemical and biological systems, *Rev. Mod. Phys.* 2002, 74, 329-345.
- (18) Gerelli, Y.; Barbieri, S.; Di Bari, M.T.; Deriu, A.; Cantù, L.; Brocca, P.; Sonvico, F.; Colombo, P.; May, R.; Motta, S. Structure of self-organized multilayer nanoparticles for drug delivery. *Langmuir* 2008, 24, 11378-11384
- (19) Souto, E.B.; Mehnert, W.; Müller, R.H. Polymorphic behaviour of Compritol®888 ATO as bulk lipid and as SLN and NLC. *J. Microencapsul.* 2006, 23, 417-433.

- (20) Souto, E.B.; Müller, R.H. SLN and NLC for topical delivery of ketoconazole. *J Microencapsul.* 2005, 22, 501-10.
- (21) Brubach, J.B.; Jannin, V.; Mahler, B.; Bourgaux, C.; Lessieur, P.; Roy, P.; Ollivon, M. Structural and thermal characterization of glyceryl behenate by X-ray diffraction coupled to differential calorimetry and infrared spectroscopy. *Int J Pharm.* 2007, 336, 248-56
- (22) Boucard, N.; David, L.; Rochas, C.; Montembault, A.; Viton, C.; Domard, A. Polyelectrolyte Microstructure in Chitosan Aqueous and Alcohol Solutions, *Biomacromol.* 2007, 8, 1209–121
- (23) Bonferoni, M.C.; Sandri, G.; Rossi, S.; Ferrari, F.; Caramella, C. Chitosan and its salts for mucosal and transmucosal delivery. *Expert Opin. Drug Del.*, 2009, 6, 923-939
- (24) Sandri, G.; Rossi, S.; Bonferoni, M.C.; Ferrari, F.; Mori, M.; Caramella, C. The role of chitosan as a mucoadhesive agent in mucosal drug delivery, *J. Drug Del. Sci. Technol.*, 2012, 22, 275-284
- (25) Sandri, G.; Bonferoni, M.C.; Ferrari, F.; Rossi, S.; Mori, M.; Caramella, C. Opportunities offered by chitosan-based nanotechnology in mucosal/skin drug delivery, *Curr. Top. Med. Chem.*, 2015, 15, 401-12
- (26) Rossi, S.; Ferrari, F.; Bonferoni, M.C.; Caramella, C. Characterization of chitosan hydrochloride-mucin interaction by means of viscosimetric and turbidimetric measurements, *Eur. J. Pharm. Sci.* 2000, 10, 251-257

Figures

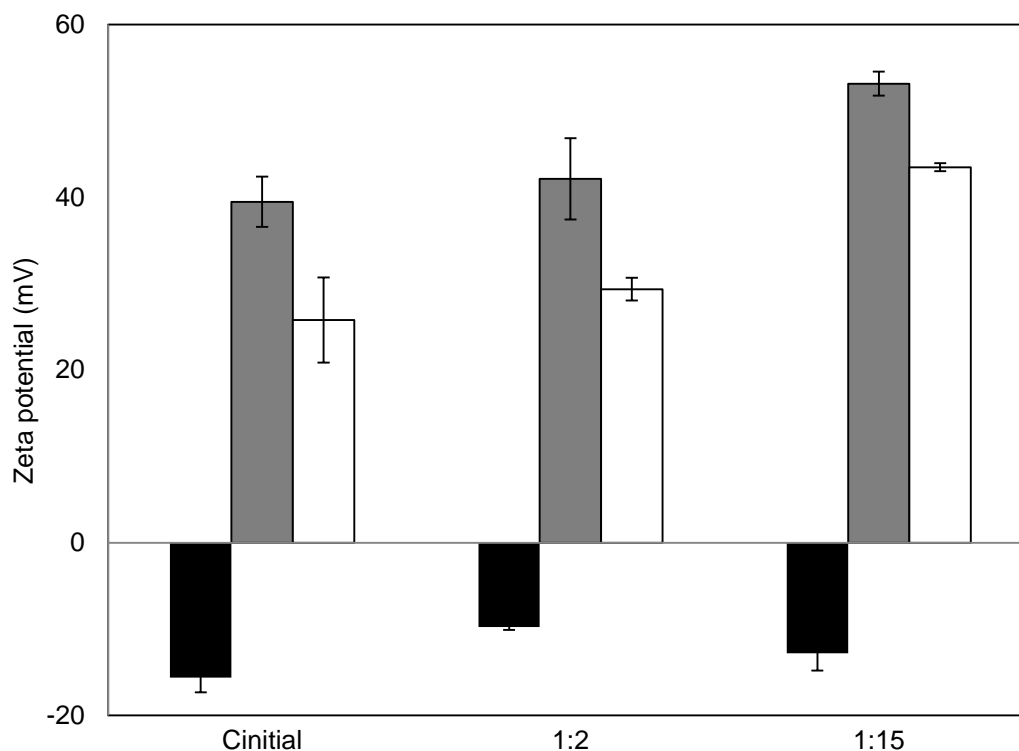


Figure 1. Zeta Potential of nanoparticles systems at different concentration. Cinitial is the concentration of the solutions as from the preparation protocol, then submitted to 2-fold and 15-fold dilution. SLNs (black), CS-SLNs (gray), CS-c-SLNs (white). Chitosan-free nanoparticles bear negative charge. Chitosan-associated nanoparticles bear a positive charge systematically higher than chitosan-covered ones.

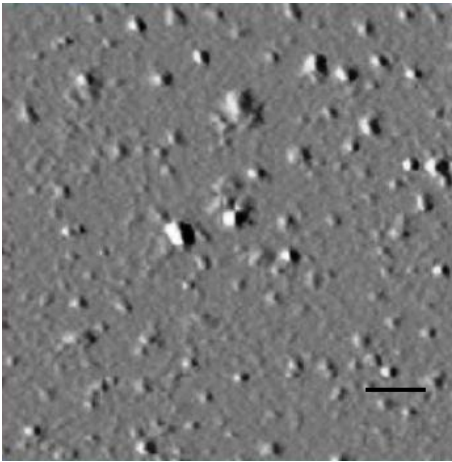


Figure 2. Morphology of SLN nanoparticles in the chitosan-free system. Bar is 200 nm.

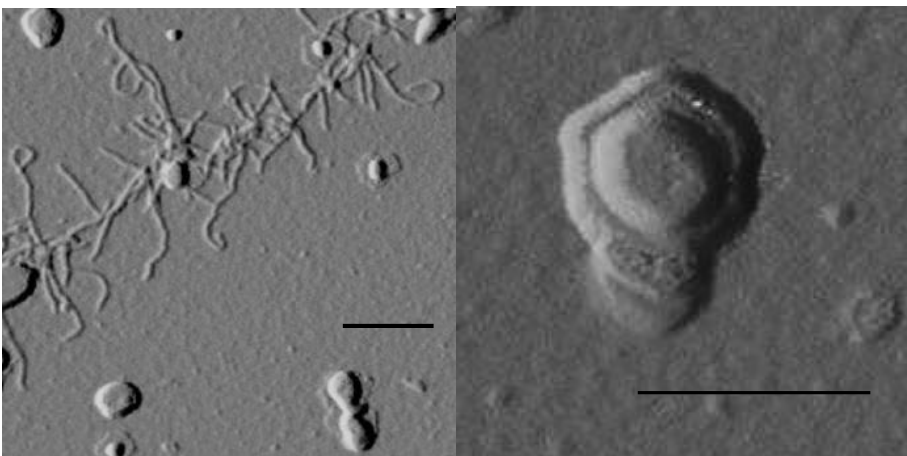


Figure 3. Morphology of nanoparticles in the CS-SLN chitosan-based system. Left Panel: In this AFM image it was possible to catch simultaneously some chitosan-based CS-SLNs nanoparticles, as well as residual free chitosan and small chitosan-free particles. The overall number distribution of this image is not representative of the whole solution, being the largely predominant population that of the CS-SLNs. Right panel: sometimes chitosan-associated CS-SLNs particles show up to have faceted morphology. Bar is 200 nm.

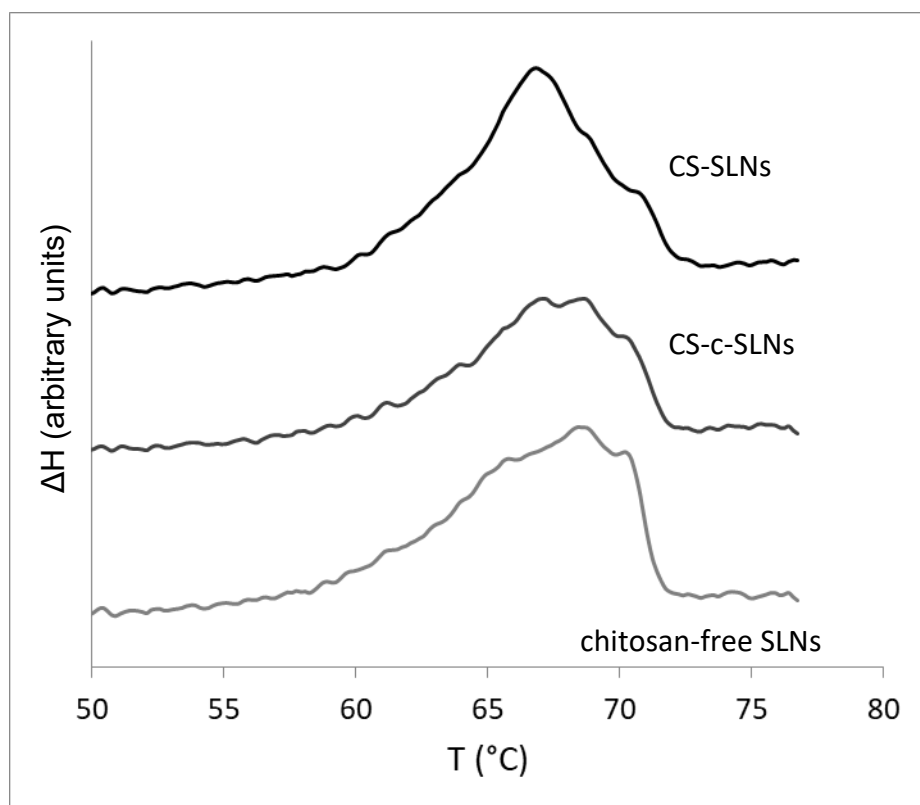


Fig. 4 DSC of nanoparticles. The DSC profiles of the second heating scans, collected at a scan rate of 1°C/min, are reported (from bottom) for chitosan-free SLNs, CS-c-SLNs and CS-SLNs, vertically shifted for better clarity. The three components found for bulk Compritol® can be recognized also in nanoparticles.

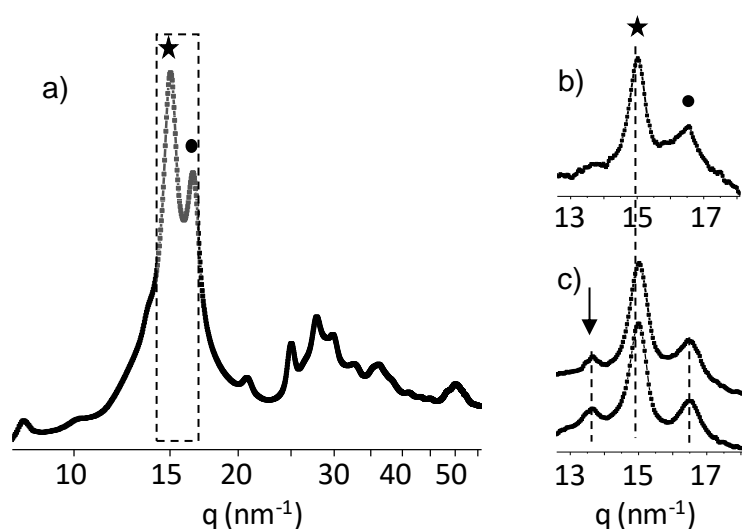


Fig. 5. WAXS spectra. a) Compritol®, b) SLNs, c) CS-SLNs and CS-c-SLNs, vertically shifted for clarity. The two major peaks are centered at $q = 15 \text{ nm}^{-1}$ (star) and $q = 16.5 \text{ nm}^{-1}$ (circle). In the Cs-SLNs and CS-c-SLNs spectra, an additional peak rises, at $q = 13.6 \text{ nm}^{-1}$, marked by an arrow. In

panels b) and c) a smaller q -range of the spectra is reported as compared to panel a).

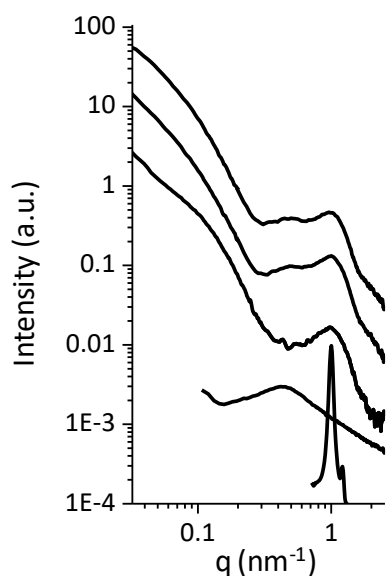


Fig. 6. SAXS spectra. From top: CS-c-SLNs , CS-SLNs and SLNs, vertically shifted for clarity. At the bottom, a significative portion of the spectra of pure Compritol® (showing a characteristic sharp peak around $q = 1 \text{ nm}^{-1}$) and of pure chitosan (with a broad peak centered at $q = 0.43 \text{ nm}^{-1}$) are reported, to facilitate identification of components contribution.

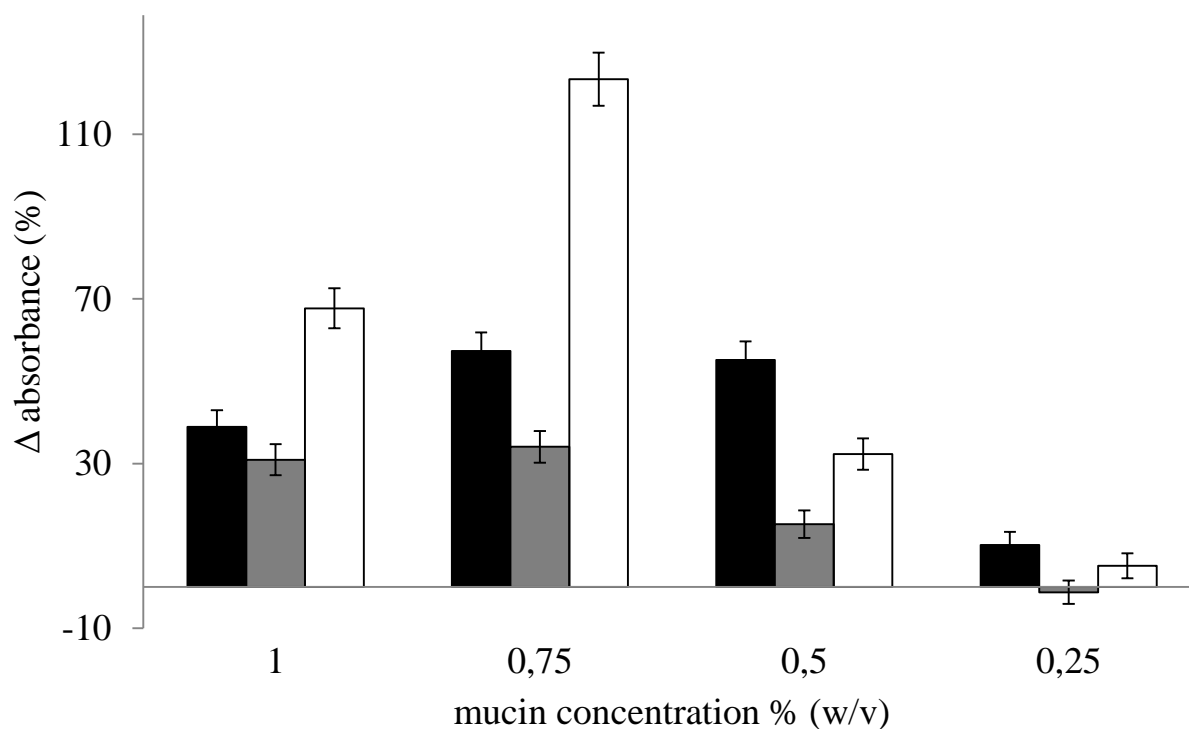


Fig. 7. Mucoadhesion. Percent excess absorbance of mucin admixed with CS-SLN (black), CS-c-SLN (gray) and pure chitosan (white).

SUPPORTING MATERIAL

Differential Scanning Calorimetry.

DSC of Compritol[®]

The predominant contribution in the DSC scans on the SLNs is given by the Compritol[®] 888ATO, which is an atomized mixture of glycerol mono- (18% bw), di- (52% bw) and tri-behenate (28% bw) (Ph. Eur.).

Along the melting process, the heterogeneous and polymorphic nature of Compritol[®] results in a complex DSC thermogram reported in Fig. SM1, left panel.

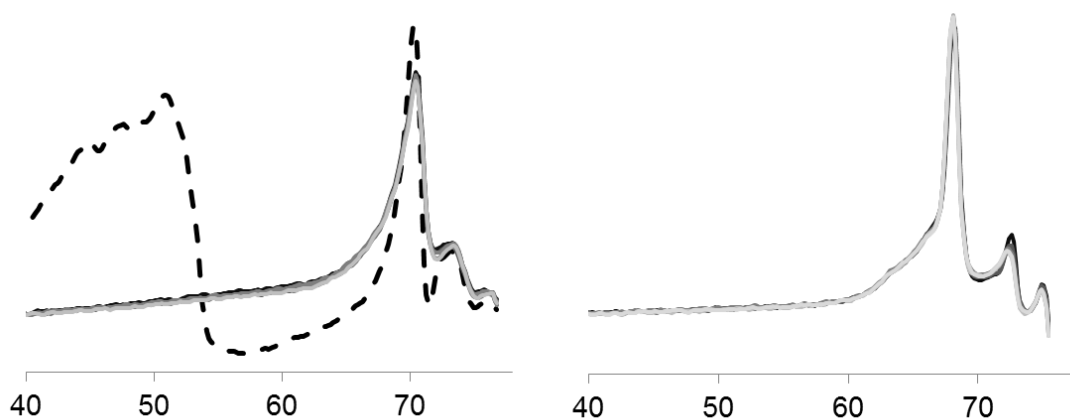


Fig. SM1. DSC of Compritol[®] *Left panel:* heating scans, melting process. Dashed line is first scan. Five more subsequent scans are reported, nearly superimposable. *Right panel:* cooling scans, recrystallization process. Six subsequent scans are reported, nearly superimposable.

The thermogram relative to the first heating run, the only one before any melting, is different from all the others. It shows a melting event at 70.3 °C and an endothermic broad peak, around 48°C. The peak at lower temperature corresponds to the melting of the α -variety, an unstable structure in Compritol[®] that disappears after the first melting (19). The melting event at high temperature shows a superposition of peaks relative to different components of the Compritol[®] mixture. In fact, three peaks are identified on melting: the main at 70.4°C, an intermediate one at 73.1°C, and a small one at higher temperature, >75°C.

DSC on chitosan-free SLNs and chitosan-coupled SLNs

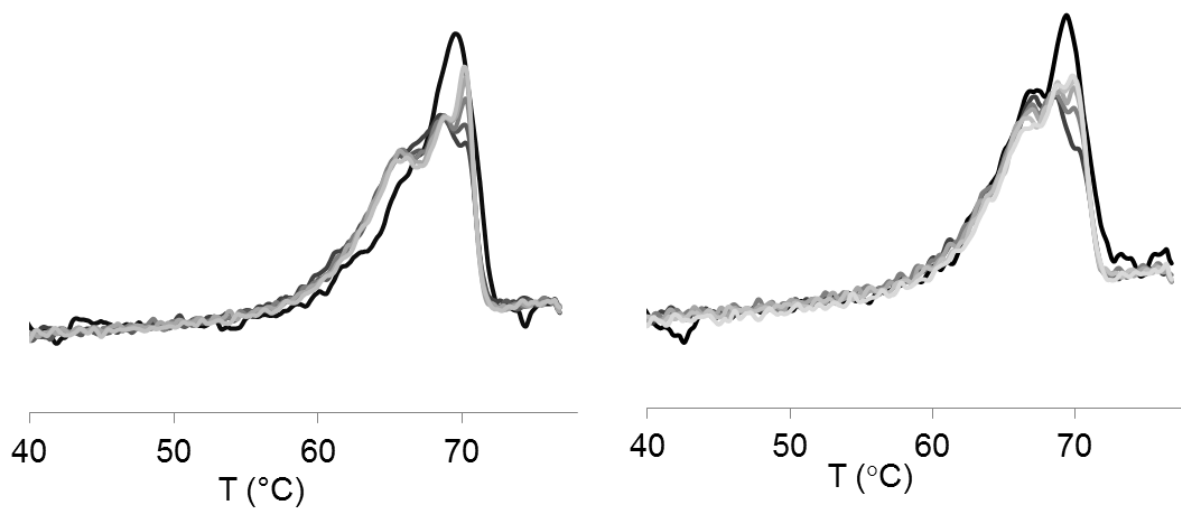


Fig. SM2. DSC thermograms of CS-SLNs

Heating scans are reported. *Left panel:* chitosan-free SLNs. *Right panel:* CS-SLNs. Six subsequent scans are reported, from dark to light, showing structural evolution.